OPEN ACCESS

Scholars International Journal of Chemistry and Material Sciences

Abbreviated Key Title: Sch Int J Chem Mater Sci
ISSN 2616-8669 (Print) |ISSN 2617-6556 (Online)
Scholars Middle East Publishers, Dubai, United Arab Emirates
Journal homepage: http://saudijournals.com

Original Research Article

Nitrosopyrazolone Metal Complexes, Synthesis, Characterization and Biological Studies

Nasir Abbas[1*], Syed Ahmad Tirmizi[3], Ghulam Shabir[3], Aamer Saeed[3], Zobia Yaseen[2], Sadia Saleem[2], Muqeet ur Rehman[2], Muhammad Imtiaz[2], Ali Bahadur[3], Muhammad Nadeem Akhtar[1]

[1]Department of Chemistry, Ghazi University Dera Ghazi Khan, 32200, Pakistan
[2]Department of Chemistry, University of Agriculture Faisalabad, 38000, Pakistan
[3]Department of Chemitry, Quaid-i-Azam University Islamabad, 45320, Pakistan

DOI: 10.36348/sijcms.2021.v04i06.001 | **Received:** 10.06.2021 | **Accepted:** 13.07.2021 | **Published:** 17.07.2021

***Corresponding author:** Nasir Abbas

Abstract

The current work deals with the synthesis of Nitrosopyrazolones and their metal complexes with some transition metals. These were then characterized by various spectroscopic techniques like UV-Visible, FT-IR, ^{1}H and ^{13}C-NMR. Electrochemical studies were conducted in order to rationalize their redox behavior. These were then screened against Hep-G2 cancer cell line showing promising results.

Keywords: Nitrosopyrazolones, spectroscopic techniques, electrochemical studies, Hep-G2 cell line.

INTRODUCTION

1. Nitrosopyzolones

Nitrosopyrazolones has enormous use in various industries as pigments. They have the ability to exhibit the chelates with various transition metal ions. These are used as analytical reagents. They are characterized by their high stability due to the formation of six membered ring. Some metal complexes are found to be more anti-inflammatory drugs than their relative ligands. The biological implications have attracted the great deal of interest primarily due to pyrazolone derived ligands. The pyrazole based ligands having O donors are reported to be anticarcinogenic and antiviral owing to their efficacy [1-3].

Depending on the previous studies pyrazolone derivatives have profound biological activity. It has been noticed that Cu (II) complexes of 1-phenyl-3-methyl-4-benzoyl-5-pyzolones as anti-inflammatory drugs are often more active than the parent ligands themselves [4]. In recent years several works have appeared concerning models of copper enzymes [5, 6].

This growing trend in mimicking the active sites of metalloproteins has a major contribution to the development of new ideas and trends in coordination chemistry. The coordination chemistry of pyrazole derived ligands has received much attention, primarily due to their biological implications. Several studies have centered around the the synthesis and structural studies of metal complexes of pyrazole containing bidentate ligands (N, O donors) due to the reported anticarcinogenic and antiviral activity of these donor ligands and complexes obtained from them. The coordination chemistry of Zn is of considerable interest [7].

The active binding sites of zinc could be applied in highly efficient and catalytic reactions by using a variety of coordination possibilities such as variability and flexibility of ligands in biologically relevant coordination spheres [8]. Since changes in coordination geometery due to the flexibility of binding ability of ligands can lead to an open position at the metal ion site, these may be beneficial for catalytic reactions to occur [9]. The ligands containing imidazole or substituted imidazole groups, similar to pyrazole or substituted pyrazole groups are known to occur in metalloproteins [10].

Recently, several metal complexes containing N, S and N, O donors have been synthesized and studied [11-13, 13]. This may be due to the reported anticarcinogenic and antiviral activity of these donor ligands and complexes obtained from them [13, 14]. It has been reported that substituted pyrazolones, pyrazolines and pyrazoles have potential biological activity [15, 16]. Derivatives of 2-pyrazolines-5-ones

have been studied for their importance as antipyretics and analgesics [17]. 5-pyrazolones and their nitroso derivatives have been found to be effective germicides and fungicides [16]. Several complexes of Schiff base derived from 2-pyrazolines-5-ones have been reported [18, 19].

However reports on Ruthenium (II) complexes containing bidentate Schiff bases derived from 5-pyrazolones seems to be rare. Gopinathan et al, have reported the synthesis of ruthenium (II) Schiff base complexes derived from aromatic aldehydes and ketones. Good fungicidal and germicidal properties have been studied about the nitroso pyrazolones [20].

Nitroso compounds used as free radical scavengers. The only nitroso dye of commercial importance is the iron complexes of 1-nitroso-2-naphthol and its sulpho derivatives. Six membered chelates formation actually corresponds to the stability of the formed metal complexes.

MATERIALS AND METHODS

All the chemicals were purchased from BDH, Sigma Aldrich. Analytical grade solvents were used. These include $MnCl_2.4H_2O$, $FeSO_4.7H_2O$, $CoCl_2.6H_2O$, $NiCl_2.6H_2O$, $CuCl_2.2H_2O$, Zn $(CH_3COO)_2$. $2H_2O$, Cd $(CH_3COO)_2.2H_2O$, $Hg(CH_3COO)_2$ and $PdCl_2$. Triethylamine, Sodium nitrite, ethanol, Methanol, deuterated dimethyl sulfoxide, ethylacetoacetate.

Melting points were determined in an open capillary tube on Gallenkamp UK.The IR spectra were run on Cary (FTIR). Similarly UV of all the samples were run in distilled water at Schimadzu-UV 1700 in distilled water. The ^{1}HNMR and ^{13}C-NMR spectra were recorded in CH_3OH using NMR Bruker DPX 400 spectrophotometer operating at 300 MHz. The internal standard used was TMS and chemical shift (δ) in ppm. The PH was monitored using portable PH meter Model (PHB4). Silica gel based TLC plates were employed using peteroleum ether: methanol 1:9 v/v as the eluting solvent. The developed plates were visualized using a UV lamp for the presence of spots and R_f values were properly calculated. Cyclic Voltametric studies, DNA binding studies and anticancer studies were employed.

2. General procedure for the synthesis of 1-phenyl-3-methyl-4-nitroso-5-pyrazolone

1-phenyl-3-methyl-4-nitroso-5-pyrazolones; m.p 195-200℃ was prepared as follows, the nitrosation reaction was carried out by acidifying the cooled aqueous solution of 1-phenyl-3-methyl-4-nitroso-5-pyrazolones (0.2 mol) at 0℃ in sodium hydroxide solution containing equivalent amount of sodium nitrite (0.2 mol) with hydrochloric acid the precipitated compound was filtered off washed several with in water and recrystallized from ethanol. The purity of this ligand was determined from results of elemental analysis, IR, ^{1}H NMR. The resulting nitroso compound has the following structure.

2.1. Metallization of 2

The 1:2 and 1:3 chelates were prepared by mixing a hot alcoholic solution of the ligand under investigation (0.0004 mol) with calculated (0.0004 mol) of metal salts solution. The reaction mixture was refluxed for 4 h. The pH of the solution was maintained at a value of 5.0-6.0 by the addition of dilute triethylamine solution. The solid product was dried in vacuum desiccator.

($C_{10}H_9N_3O_2$) (2)

Yellow, (71%) λ_{max} (nm): 397. FTIR (KBr, cm^{-1}) ν_{max}: 3464 (OH str.), 3181 (C=C-H str.), 2760 (CH_2 str.), 1703 (C=O str.), 1593, 1501 (C=C aromatic, C=N), 1489 (N=N str.), 1371, 1198 (C-C, C-O str.), 887 (Ar-H). ^{1}HNMR (300 MHz, DMSO-d_6) δ: 7.87 (2H, d J=7.8 Hz), 7.42 (2H, d J=7.8 Hz), 7.2 (1H, t), 2.46, 2.26 (3H, s).^{13}C-NMR (75 MHz DMSO-d_6) δ (ppm):160.42, 152.22, 148.85, 144.1, 142.42, 137.71, 128.43, 125.03, 118.38, 16.06, 11.01. Anal. Calcd. For **$C_{10}H_9N_3O_2$:** C, 59.11; H, 4.46; N, 20.68; O, 15.75; Found: C, 59.05; H, 4.30; N, 20.59; O, 15.79.

$Mn(C_{10}H_9N_3O_2)_3$ (4a)

Greyish green, (80%). λ_{max} (nm): 393. FTIR (KBr, cm^{-1}) ν_{max}: 3080 (CH_2 str.), 1634 (C=O str.), 1500, 1371 (C=C aromatic, C=N), 1400, 1198 (C-O str.), 1071 (C-OC str.), 896 (Ar-H bend). Anal. Calcd. For **$C_{30}H_{24}MnN_9O_6$:** C, 54.47; H, 3.66; Mn, 8.30; N, 19.06; O, 14.51; Found: C, 54.78; H, 3.20; N, 19.58, O, 14.57.

$Fe\ (C_{10}H_9N_3O_2)_3$ (4b)

Dark Green, (78%). λ_{max} (nm): 308. FTIR (KBr, cm^{-1}) ν_{max}: 3076 (C=C-H str.), 1619, 1597 (C=C aromatic), 1215, 1146 (C-O str.C-N), 909 (Ar-H bend).).Anal. Calcd. For **$C_{30}H_{24}FeN_9O_6$:** C, 54.40; H, 3.65; Fe, 8.43; N, 19.03; O, 14.49; Found: C, 54.24; H, 3.41; N, 19.21, O, 14.04.

$Co\ (C_{10}H_9N_3O_2)_3$ (4c)

Brownish Grey, (81%). λ_{max} (nm): 309. FTIR (KBr, cm^{-1}) ν_{max}: 3060 (C=C-H str.), 1627 (C=C str.), 1619, 1541 (C=C aromatic), 1373 (CH_2 str.), 1215 (C-O str.), 1148 (C-N), 840 (Ar-H). Anal. Calcd. For **$C_{30}H_{24}CoN_9O_6$:** C, 54.14; H, 3.63; Co, 8.86; N, 18.94; O, 14.42: Found: C, 54.37; H, 3.69; N, 18.96; O, 12.54.

$Ni\ (C_{10}H_9N_3O_2)_3$ (4d)

Light Green, (80%). λ_{max} (nm): 314. FTIR (KBr, cm^{-1}) ν_{max}: 3080 (C=C-H str.), 2926 (CH_2 str.), 1630, 1586 (C=C aromatic, C=N), 1218, 1146 (C-O str. C-N), 911 (Ar-H). Anal. Calcd. For **$C_{30}H_{24}N_9NiO_6$:** C, 54.16; H, 3.64; N, 18.95; Ni, 8.82; O, 14.43; Found: C, 54.46; H, 3.31; N, 18.56; O, 14.80.

$Cu(C_{10}H_9N_3O_2)_3$ (4e)

Green, (77%). λ_{max} (nm): 316. FTIR (KBr, cm^{-1}) ν_{max}: 2922 (C=C-H str.), 1618 (C=C aromatic), 1377, 1140, 1075 (C-C str, C-N), 872 (Ar-H). Anal. Calcd. For **$C_{30}H_{24}CuN_9O_6$:** C, 53.77; H, 3.61; Cu, 9.48; N, 18.81; O, 14.33; Found: C, 53.35; H, 3.13; Cu, 9.15; N, 18.04; O, 14.20.

$Zn(C_{10}H_9N_3O_2)_3$ (4f)

Light Yellow, (82%). λ_{max} (nm): 310. FTIR (KBr, cm^{-1}) ν_{max}: 3076 (C=C-H str.), 1632 (C=C aromatic), 1489 (C=N str.), 1217, 1071 (C-C str.), 911 (C-N str.), 888 (C-O str.), 754 (Ar-H).). Anal. Calcd. For **$C_{30}H_{24}N_9O_6Zn$:** C, 53.62; H, 3.60; N, 18.76; O, 14.29; Zn, 9.73; Found: C, 53.27; H, 3.13; N, 14.04; O, 14.20; Zn, 9.57.

$Cd(C_{10}H_9N_3O_2)_2$ (4g)

Dark Yellow, (79%). λ_{max} (nm): 311. FTIR (KBr, cm^{-1}) ν_{max}: 2929 (C=C-H str.), 1623 (C=C aromatic), 1487 (C=N str.), 1373, (C-C str.), 1144 (C-N str.), 1047 (C-O str.), 998 (Ar-H).). Anal. Calcd. For **$C_{20}H_{16}CdN_6O_4$:** C, 50.12; H, 3.36; Cd, 15.63; N, 17.53; O, 13.35; Found: C, 50.35; H, 3.13; Cd, 15.28; N, 17.04; O, 13.26.

$Hg(C_{10}H_9N_3O_2)_2$ (4h)

Brick Red, (70%). λ_{max} (nm): 321. FTIR (KBr, cm^{-1}) ν_{max}: 2998 (C=C-H str.), 1645 (C=C aromatic), 1589 (C=N str.), 1362, (C-C str.), 1187 (C-N str.), 1008 (C-O str.), 907 (Ar-H). Anal. Calcd. For **$C_{20}H_{16}HgN_6O_4$:** C, 44.64; H, 3.00; Hg, 24.85; N, 15.62; O, 11.89; Found: C, 44.35; H, 3.13; Hg, 24.71; N, 15.04; O, 11.45.

$Pd(C_{10}H_9N_3O_2)_2$ (4i)

Brown, (73%). λ_{max} (nm): 318. FTIR (KBr, cm^{-1}) ν_{max}: 2920 (C=C-H str.), 1664 (C=C aromatic), 1595 (C=N str.), 1272, (C-C str.), 1187 (C-N str.), 1002 (C-O str.), 902 (Ar-H). Anal. Calcd. For **$C_{20}H_{16}PdN_6O_4$:** C, 50.54; H, 3.39; N, 17.68; O, 13.46; Pd, 14.93; Found: C, 50.56; H, 3.45; N, 17.04; O, 13.34; Pd, 14.87.

3. General procedure for the synthesis of p-methyl-1-phenyl-3-methyl-4-nitroso-5-pyrazolone.

p-methyl-1-phenyl-3-methyl-4-nitroso-5-pyrazolones; m.p 165-170℃ was prepared as follows, the nitrosation reaction was carried out by acidifying the cooled aqueous solution of p-methyl-1-phenyl-3-methyl-4-nitroso-5-pyrazolones (0.2 mol) at 0℃ in sodium hydroxide solution containing equivalent amount of sodium nitrite (0.2 mol) with hydrochloric acid the precipitated compound was filtered off washed several with in water and recrystallized from ethanol. The purity of this ligand was determined from results of elemental analysis, IR, ^{1}H NMR. The resulting nitroso compound has the following structure.

3.1. Metallization of 6

The 1:2 and 1:3 chelates were prepared by mixing a hot alcoholic solution of the ligand under investigation (0.0004 mol) with calculated (0.0004 mol) of metal salts solution. The reaction mixture was refluxed for 4 h. The pH of the solution was maintained at a value of 5.0-6.0 by the addition of dilute triethylamine solution. The solid product was dried in vacuum desiccator

$(C_{11}H_{12}N_3O_2)$ (6)

Yellow, (71%) λ_{max} (nm): 397. FTIR (KBr, cm^{-1}) ν_{max}: 3520 (OH str.), 3140 (C=C-H str.), 2919 (CH_2 str.), 1684 (C=O str.), 1611, 1507 (C=C aromatic, C=N), 1367, 1196 (C-C, C-O str.), 881 (Ar-H). ^{1}HNMR (300 MHz, DMSO-d_6) δ: 7.71 (1H, d J=8.4 Hz), 7.21 (1H, d J=8.4 Hz), 2.44 (3H, s), 2.24 (3H, s).^{13}C-NMR (75 MHz DMSO-d_6) δ (ppm):160.26, 152.07, 148.66, 144.14, 142.22, 135.30, 134.98, 128.91, 118.57, 19.58, 16.04, 10.98. Anal. Calcd. For **$C_{11}H_{12}N_3O_2$:** C, 60.54; H, 5.54; N, 19.25; O, 14.66. Found: C, 60.11; H, 5.33; N, 19.51; O, 14.22.

$Mn(C_{11}H_{12}N_3O_2)_3$ (8a)

Greyish green, (77%). λ_{max} (nm): 393. FTIR (KBr, cm^{-1}) ν_{max}: 3072 (CH_2 str.), 1678 (C=O str.), 1501, 1373 (C=C aromatic, C=N), 1196 (C-O str.), 1077 (C-O str.), 898 (Ar-H bend). Anal. Calcd. For **$C_{33}H_{33}MnN_9O_6$:** C, 56.09; H, 4.71; Mn, 7.77; N, 17.84; O, 13.59; Found: C, 56.43; H, 4.45; N, 17.78, O, 13.51.

Fe $(C_{11}H_{12}N_3O_2)_3$ (8b)

Dark Green, (75%). λ_{max} (nm): 308. FTIR (KBr, cm^{-1}) ν_{max}: 3069 (C=C-H str.), 1629, 1599 (C=C aromatic), 1225, 1158 (C-O str.C-N), 919 (Ar-H bend).).Anal. Calcd. For **$C_{33}H_{33}FeN_9O_6$:** C, 56.02; H, 4.70; Fe, 7.89; N, 17.82; O, 13.57; Found: C, 56.32; H, 4.67; N, 17.76, O, 13.46.

Co $(C_{11}H_{12}N_3O_2)_3$ (8c)

Brownish Grey, (78%). λ_{max} (nm): 309. FTIR (KBr, cm^{-1}) ν_{max}: 3068 (C=C-H str.), 1632 (C=C str.), 1627, 1552 (C=C aromatic), 1383 (CH_2 str.), 1225 (C-O str.), 1157 (C-N), 850 (Ar-H). Anal. Calcd. For **$C_{33}H_{33}CoN_9O_6$:** C, 55.78; H, 4.68; Co, 8.29; N, 17.74; O, 13.51. Found: C, 55.62; H, 4.66; N, 17.78; O, 13.47.

Ni $(C_{11}H_{12}N_3O_2)_3$ (8d)

Light Green, (80%). λ_{max} (nm): 314. FTIR (KBr, cm^{-1}) ν_{max}: 3085 (C=C-H str.), 2930 (CH_2 str.), 1641, 1589 (C=C aromatic, C=N), 1229, 1153 (C-O str. C-N), 922 (Ar-H). Anal. Calcd. For $C_{33}H_{33}NiN_9O_6$: C, 55.80; H, 4.68; N, 17.75; Ni, 8.26; O, 13.51; Found: C, 55.79; H, 4.33; N, 17.57; Ni, 8.34; O, 13.38.

Cu $(C_{11}H_{12}N_3O_2)_3$ (8e)

Green, (74%). λ_{max} (nm): 316. FTIR (KBr, cm^{-1}) ν_{max}: 2931 (C=C-H str.), 1622 (C=C aromatic), 1382, 1153, 1085 (C-C str, C-N), 882 (Ar-H). Anal. Calcd. For **$C_{33}H_{33}CuN_9O_6$:** C, 55.42; H, 4.65; Cu, 8.88; N,

17.63; O, 13.42; Found: C, 55.34; H, 4.32; Cu, 8.23; N, 17.18; O, 13.27.

Zn ($C_{11}H_{12}N_3O_2)_3$ (8f)

Light Yellow, (79%). λ_{max} (nm): 310. FTIR (KBr, cm^{-1}) ν_{max}: 3078 (C=C-H str.), 1638 (C=C aromatic, 1227, 1079 (C-C str.), 923 (C-N str.), 897 (C-O str.), 764 (Ar-H).). Anal. Calcd. For **$C_{33}H_{33}ZnN_9O_6$:** C, 55.27; H, 4.64; N, 17.58; O, 13.39; Zn, 9.12; Found: C, 55.24; H, 4.45; N, 17.42; O, 13.20; Zn, 9.29.

Cd($C_{11}H_{12}N_3O_2)_2$ (8g)

Dark Yellow, (76%). λ_{max} (nm): 311. FTIR (KBr, cm^{-1}) ν_{max}: 2929 (C=C-H str.), 1623 (C=C aromatic), 1487 (C=N str.), 1373, (C-C str.), 1144 (C-N str.), 1047 (C-O str.), 991 (Ar-H).). Anal. Calcd. For **$C_{22}H_{22}CdN_6O_4$:** C, 51.87; H, 4.35; Cd, 14.71; N, 16.50; O, 12.56; Found: C, 51.79; H, 4.19; Cd, 14.39; N, 16.28; O, 12.19.

Hg($C_{11}H_{12}N_3O_2)_3$ (8h)

Brick Red, (67%). λ_{max} (nm): 321. FTIR (KBr, cm^{-1}) ν_{max}: 2920 (C=C-H str.), 1650 (C=C aromatic), 1506 (C=N str.), 1370, (C-C str.), 1176 (C-N str.), 1095 (C-O str.), 1003 (Ar-H). Anal. Calcd. For **$C_{22}H_{22}HgN_6O_4$:** C, 46.51; H, 3.90; Hg, 23.54; N, 14.79; O, 11.26; Found: C, 46.31; H, 3.85; Hg, 23.36; N, 14.59; O, 11.21.

Pd($C_{11}H_{12}N_3O_2)_3$ (8i)

Brown, (70%). λ_{max} (nm): 318. FTIR (KBr, cm^{-1}) ν_{max}: 2921 (C=C-H str.), 1667 (C=C aromatic), 1598 (C=N str.), 1278, (C-C str.), 1189 (C-N str.), 1002 (C-O str.), 909 (Ar-H). Anal. Calcd. For $C_{22}H_{22}PdN_6O_4$: C, 52.28; H, 4.39; N, 16.63; O, 12.66; Pd, 14.04; Found: C, 52.22; H, 4.31; N, 16.56; O, 12.33; Pd, 14.01.

RESULT AND DISCUSSION

4. Synthesis of pyrazolone series of chromophores.

In this series 20 chromophores were prepared. Two different pyrazolones namely (1-phenyl-3-methyl-4-nitroso-5-pyrazolones) and (p-methyl 1-phenyl-3-methyl-4-nitroso pyrazolone) were used as ligands. Nine chromophoric samples were prepared with each ligand. The first unmetallized ligand nine was Manganese, Iron, cobalt, Nickel, Copper, Zinc, Cadmium, Mercury and Palladium complexes respectively. Manganese, Nickel, Zinc, Palladium complexes were of 1:2 ratio, while Iron, Cobalt, Copper and Cadmium complexes were of 1:3 ratio. A generalized scheme for the synthesis of all type of ligands and their metal complexes was given in scheme 1.

1-phenyl-3-methyl-4-nitroso-5-pyrazolones; m.p 195-200℃ was prepared [21] as following, the nitrosation reaction was carried out by acidifying the cooled aqueous solution of 1-phenyl-3-methyl-4-nitroso-5-pyrazolones (0.2 mol) at 0℃ in sodium hydroxide solution containing equivalent amount of sodium nitrite (0.2 mol) with hydrochloric acid the precipitated compound was filtered, washed several times with water and recrystallized in ethanol. The purity of this ligand was determined from results of elemental analysis; other one remaining ligand was prepared in the same manner.

4.1 Metallization of Acid Dyes

The 1:2 and 1:3 chelate complexes were prepared by mixing a hot alcoholic solution of the ligands under investigation (0.0004 M) with calculated (0.0004 M) of metal salts solution. The reaction mixture was refluxed for 2-3 hrs. The pH of the solution was maintained at a value of 5.0-6.0 by the addition of dilute ammonia solution (1:10) or triethyl amine. The solid product was dried in a vacuum desiccator.

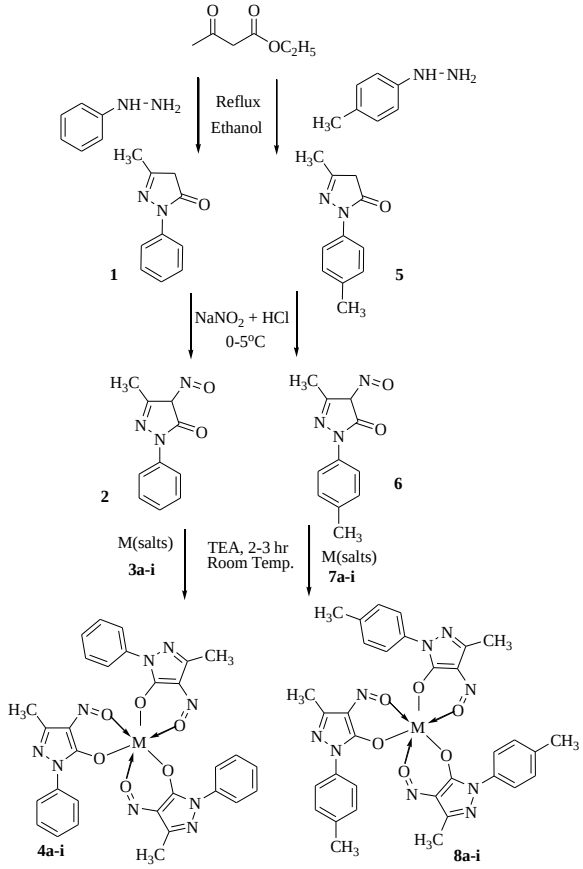

M=Mn(II) ,Fe(II), Co(II) ,Ni(II) ,Cu(II) ,Zn(II),Cd(II), Hg(II), Pd(II)

Scheme 1 Syntheses of ligand **2** and **6**, their metal complexes **4a-i** and **8a-i**

4.2 UV-Visible of pyrazolone based chromophores

The absorption maxima (λ_{max}) of ligand (2) and its metal complexes (4a-i) were recorded in DMSO and were shown in Table 1. They showed absorption maxima λ_{max} in the range of 300 to 400 nm which was due to π-π* transition in N=O which was involved in Nitroso-Oxime tautomerism. All the chromophores were of the same functionality but difference lied in the substituents present at the phenyl ring attached to the pyrazol moiety. There was a little effect on λ_{max} but prominent shifts (bathochromic and hypsochromic) on

the λ_{max} was observed in metal complexes. The UV-Visible data presented in the Table 1 could be supported by UV-visible spectra in Fig. 1. The ligand 2 was of orange yellow colour with λ_{max} at 396 nm. Its metallization with manganese changed its color to greyish green having λ_{max} at 585 (4a) showing a bathochromic shift of 189 nm with hypochromic effect. The ligand 2 complexed with metal ions 3a-i produced the pigments 4a-i. Hypsochromic/Blue shift was observed in all the complexes 4a-i as given in the table 2.1 which is upto 88 nm. 4b showed the hypsochromic shift of 88 nm with hyperchromic effect the color exhibited by the pigment was light green. Although 3b was electropositive as compared to other metal ions which were being used here for complexation and snatched the electron density from the ligand. This was the reason for the hypsochromic shift. Total nine metal ions had been employed in this series but maximum shift was observed only in 4b complex consisting of Fe^{2+}. Another interesting aspect was that the band gap between the π-π* orbitals of ligand was increased this the reason that much greater energy is required to excite the electrons in this pigment. On complexation of 2 with 3c and metal ion 4c was obtained with λ_{max} at 309 nm showing the hyperchromic effect at 0.996. This is the second complex which showed the hypsochromic shift of 87 nm. An average hypsochromic shift was being observed in case of 4d-4g which was less than the Fe^{2+} and Co^{2+} complexes. Not much difference in the shift was observed in the group IIB elements i.e Zn^{2+} and Cd^{2+} 4f and 4g. Conversely speaking 4f-4g showed less shift (75 nm) as observed in 4h complexes in which the Hg^{2+} which showed lanthanide contraction. The emitted color was red in 4h. While the reddish orange color was observed in case of 4i pigment which is obtained by complexing 2 with 3i. It was concluded from the above discussion that all the complexes except 4b showed hypsochromic shift mostly with hyperchromic effect. The geometries of the complexes were determined by slope ratio method. The curve was given in Fig. 2 for 4e.

Table-1: Physical properties of chromophores 2 and 4a-i

Compounds	Molecular Formula	Molecular Mass	Solution Color in (DMSO)	λ_{max} (nm)
2	$C_{10}H_9N_3O_2$	203	Yellow	396/0.736
4a	$Mn(C_{10}H_9N_3O_2)_3$	661	Greenish Yellow	585/0.185
4b	$Fe(C_{10}H_9N_3O_2)_3$	662	Green	308/1.18
4c	$Co(C_{10}H_9N_3O_2)_3$	665	Brownish Yellow	309/0.996
4d	$Ni(C_{10}H_9N_3O_2)_3$	665	Greenish Yellow	314/1.05
4e	$Cu(C_{10}H_9N_3O_2)_3$	669	Greenish Yellow	316/0.646
4f	$Zn(C_{10}H_9N_3O_2)_3$	670	Light Yellow	310/1.025
4g	$Cd(C_{10}H_9N_3O_2)_2$	720	Dark Yellow	311/1.22
4f	$Hg(C_{10}H_9N_3O_2)_2$	808	Brownish Yellow	321/1.062
4i	$Pd(C_{10}H_9N_3O_2)_2$	712	Reddish Yellow	318/0.617

Table-2: Stochiometeric ratios for ligand 2 with metals 3a-i

Sr. No.	Chromophore	Metals	Metal ligand Ratio	Geometery
1	**4a**	Mn^{2+}	1:3	Octahedral
2	**4b**	Fe^{2+}	1:3	Octahedral
3	**4c**	Co^{2+}	1:3	Octahedral
4	**4d**	Ni^{2+}	1:3	Octahedral
5	**4e**	Cu^{2+}	1:3	Octahedral
6	**4f**	Zn^{2+}	1:3	Octahedral
7	**4g**	Cd^{2+}	1:2	Tetrahedral
8	**4f**	Hg^{2+}	1:2	Tetrahedral
9	**4i**	Pd^{2+}	1:2	Square Planer

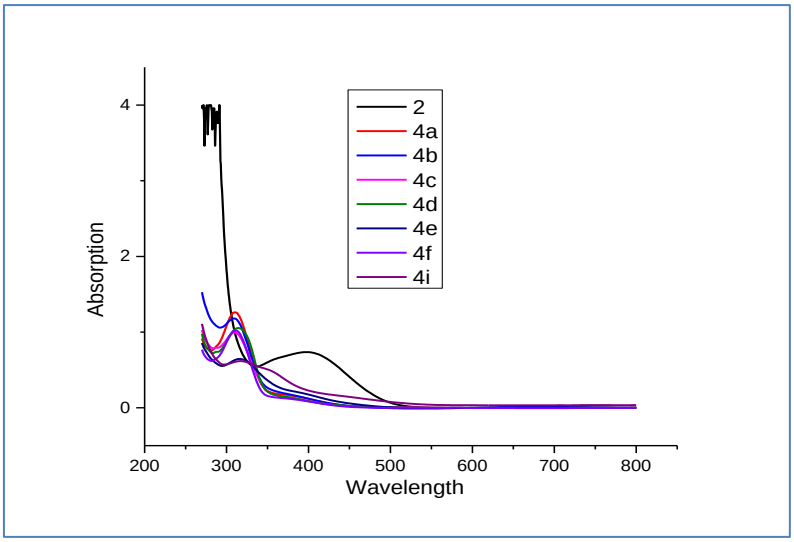

Fig-1: UV-Visible spectrum of 2 and 4a-i

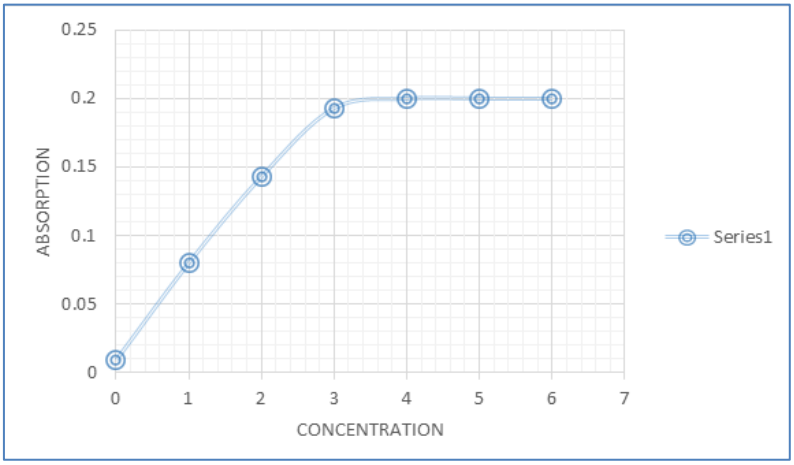

Fig-2: Slope Ratio curve for complex 4e.

4.3 FT-IR studies of pyrazolone based chromophores

The data for the 1st series of metal complexes of pyrazolone was supported by the Fig. 3 and Fig. 4 which was given below for one of the representative complex. The infrared spectra of synthesized ligand (2) and its metal complexes possessed absorption peaks due to O-H (str.3466 cm^{-1}), Ar-H (str.3198 cm^{-1}), C-H (str.2729 cm^{-1}), C=C(str.1619-1692 cm^{-1}), C=O(str.1704 cm^{-1}), N=O(str.1557-1594 cm^{-1}), C-O (str.1366-1489 cm^{-1}), C-N (str.1048 cm^{-1}), C-H (bend.1199-1310 cm^{-1}), M-O (str.511 cm^{-1}) stretching and bending vibrations. O-H (3376 cm^{-1}) as was present in the Fig.2.33 showed the hydrogen bonding in the ligand molecules. This was attributed to the fact that the ligand molecules possessed keto-oxime tautomerism, where the oxime functionality took part in hydrogen bonding. Keeping in view the spectra of compound 2 given in Fig. 3 the absorption peak at 3466 cm^{-1} was due to O-H group. A phenyl group was connected with nitrogen in the pyrazol moiety whose C-H stretching vibrations were at 3198 cm^{-1}. C=O stretch usually lied in the range of 1715-1745 cm-1, but it was observed at 1704 cm^{-1}. This was due to the phenyl ring which reduced the force constant of carbonyl functionality. The bending vibrations of methyl group were present at 1199 cm^{-1}. Synthesis of all metal complexes 4a-i were confirmed by FT-IR spectroscopy. The confirmation of the complexation was made on the basis of absorption frequencies at lower wavenumber in the range of 500-550 cm^{-1} for M-O bonding. These were not present in the spectrum of 2. One of the representative spectra for 4h was given below in Fig. 4 in which the absorption peak for M-O bond appeared at 511 cm^{-1}.

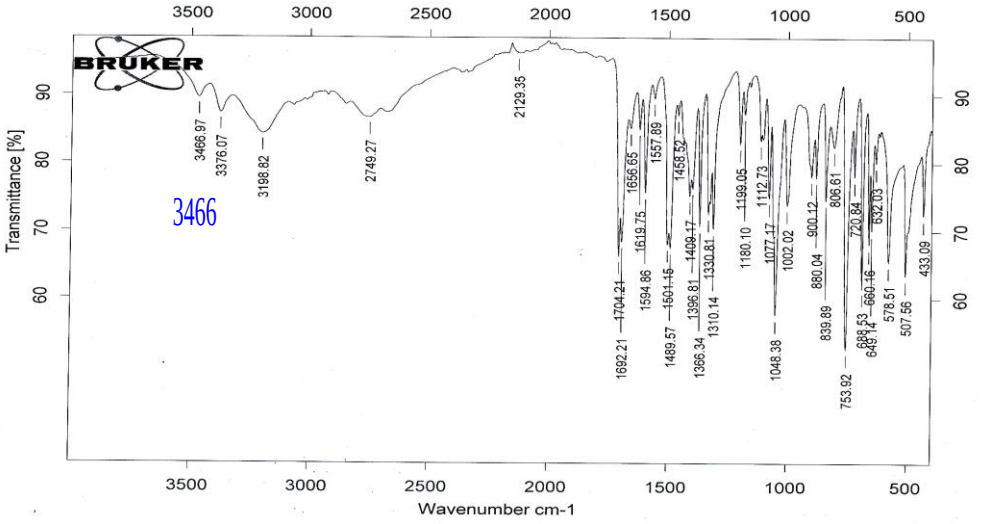

Fig-3: FT-IR spectrum of 2

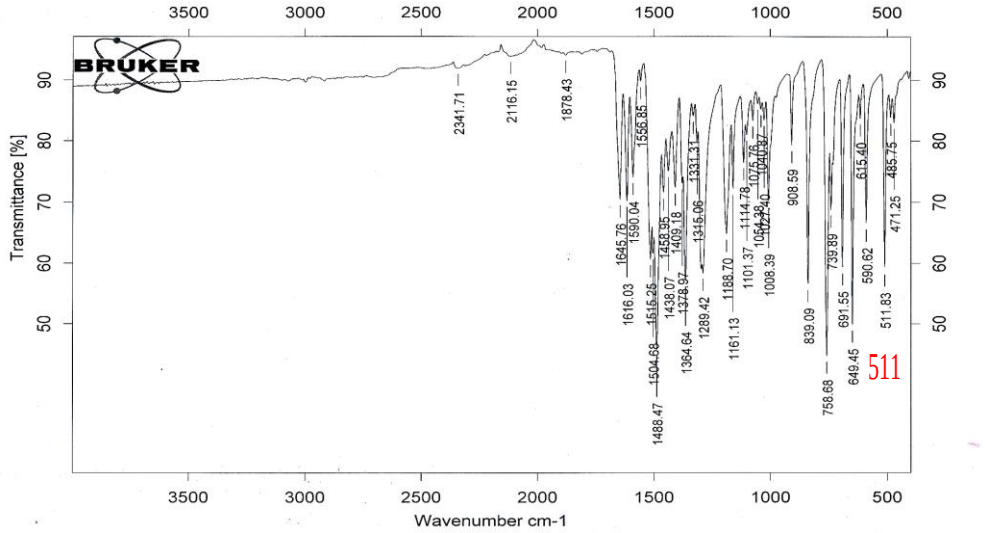

Fig-4: FT-IR spectrum of 4h

4.4 ^{1}H-NMR and ^{13}C-NMR spectroscopic elucidation of pyrazolone based chromophores

The ^{1}H-NMR and ^{13}C-NMR spectra of 2 were given in the Fig. 5 and 6 respectively. It was apparent from the ^{1}H-NMR spectrum that the ligand 2 exhibited four different kinds of chemically non-equivalent protons. Two signals were present at 2.26 and 2.46 ppm. The reason behind these two signals was due to the phenomena of keto-oxime tautomerism which was present in ligand 2. While the signals for aromatic ring were present in the de-shielded region in the range of 7.19-7.88 ppm. If we take into account splitting pattern of the aromatic protons then it was obvious that the o-protons were not only chemically equivalent but were magnetically equivalent and showing their chemical shift at 7.88 (d). This doublet was due to the neighboring proton present at the m-position. Similarly proton present at p-position of the aromatic ring was also showing its triplet signal at 7.21 ppm due to these m-protons because these are magnetically non-equivalent. However the m-protons are showing their signals at 7.41 ppm (t). More specifically speaking, ortho and m-protons were mutually coupled showing coupling constant value (J=7.8). If we consider C^{13}-NMR of the ligand 2 the aromatic peaks were present in the range of 118-128 ppm as was apparent from the Fig. 6. Signals were present at 11.01 and 16.06 ppm for methyl protons present on the pyrazol moiety. Similarly ^{13}C signal for C=O was obvious at 160 ppm. While for complexes the paramagnetic behavior of metal ions was responsible to distort the H^{1}-NMR and ^{13}C-NMR and could not be taken in to account.

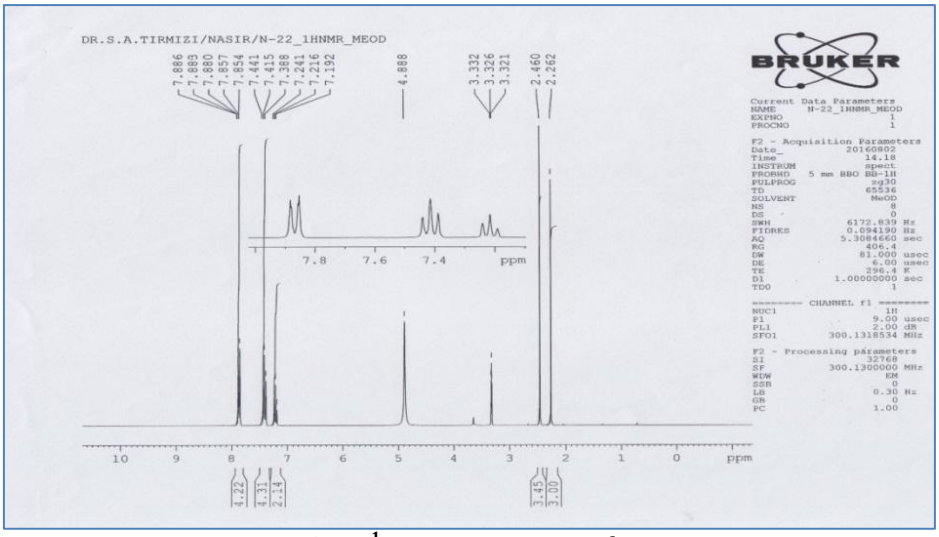

Fig-5: ^{1}H-NMR spectrum of 2.

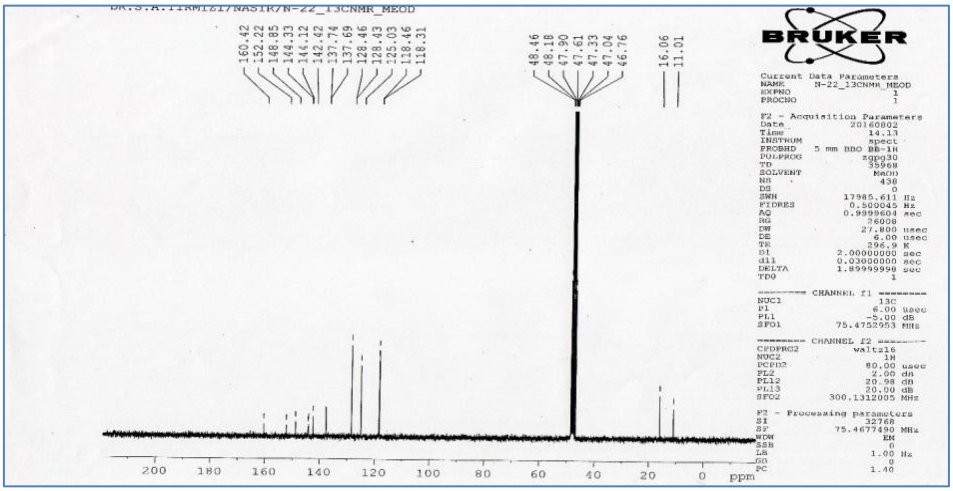

Fig-6: ^{13}C-NMR spectrum of 2.

4.5 Electrochemical studies of the pyrazolone based chromophores

Cyclic voltammetry was employed for the electrochemical characterization of the synthesized ligand 2 and 4a-i complexes as shown in Fig. 7. The supporting electrolyte was 0.1 M $TBAPF_6$ in DMSO. With the help of this technique the redox potentials i.e HOMO (highest occupied molecular orbitals) and LUMO (lowest unoccupied molecular orbitals) along with energy band gaps (Eg) were calculated.

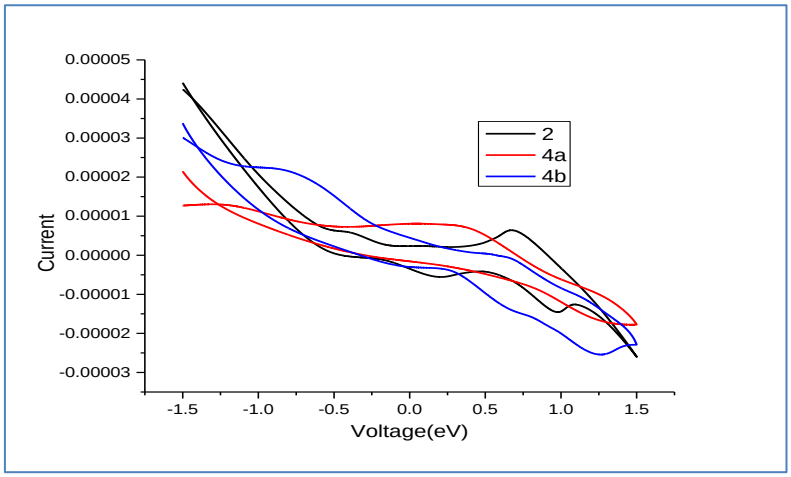

Fig-7: Cyclic Voltammogram of 2 and 4a-i

4.4.1 Redox Potentials ($E_{1/2}$)

As indicated by the cyclic voltammetric analysis of the synthesized ligand and its metal complexes exhibited their redox potentials. Oxidation and reduction potentials were calculated from the cycliv voltammogram which were given in Table 3. 4f showed the lowest redox potential while 4a possessed highest redox potential values. It was obvious from the studies that electropositive metals (Mn, E.N, 1.55) contain highest redox potential while electronegative (Zn metals have lowest redox potential.

4.4.2 Lowest Unoccupied Molecular Orbital (LUMO)

Absolute energies of the LUMO levels with respect to the vacuum level were calculated, the redox data were standardized with ferrocenne/ferricinium couple having energy -4.8 eV. The data was given in Table 3 related to LUMO level energies. The LUMO energy levels were in the range of -5.247 to -5.731 eV. It was obvious from the data that 4g contained the central metal ion which had greater van der Waals radius (158 ppm) whose impact was electron donating to the motif due to which the energy of the LUMO levels was decreased. While this was not the case with 4a whose central metal ion had less atomic radius (127pm) whose impact was electron withdrawing from the motif due to which the energy of LUMO levels was increased. Increased conjugation or delocalization of electrons decreased the energy difference in the LUMO levels and vice versa.

Table-3: LUMO energy levels of chromophores 2 and 4a-i

Sr. No.	$E_{1/2}$(V)	LUMO (eV)
2	+0.792	-5.575
4a	+0.953	-5.731
4b	+0.743	-5.349
4c	+0.910	-5.55
4d	+0.943	-5.343
4e	+0.923	-5.435
4f	+0.319	-5.321
4g	+0.435	-5.247
4h	+0.890	-5.56
4i	+0.523	-5.327

4.4.3 Band Gap Energy (Eg)

The optical band gap energies were calculated using standard procedure. Every solid had its own characteristic energy band structure. This variation in band structure was responsible for the wide range of electrical properties observed in various materials [22]. Band gap energy lies in the range of 2.29 to -3.02. Band gap energies were found to be low for 4g and high for the ligand 2. This contradiction arised due to the involvement of Cd metal which has some kind of electron releasing or back donation effect due to which the electron density on the ligand moiety increased and caused the decrease in the band gap energy in 4g while this was not the case with 2.

4.4.4 Highest Occupied Molecular Orbitals

The data related to the highest occupied molecular orbitals was given in Table 4 which was calculated by making use of Bredas equation. The energy lied in the range -7.735 to -8.596 for HOMO. The energy levels for 4g were high while these were low for 2. This discrepancy in energy was due to the fact that metal ions were responsible for dragging the electron density from ligand molecules. So HOMO energy levels were increased for the metal complexes. The maximal increment was observed in case of 4g as compared to other metal complexes and ligand 2 as presented below in Table 4.

Table-4: HOMO energy levels and band gap energy of chromophores 2 and 4a-i

Sr. No.	Eg(V)	HOMO (eV)
2	3.02	-8.596
4a	2.56	-8.291
4b	2.63	-7.93
4c	2.76	-8.31
4d	2.43	-7.773
4e	2.69	-8.125
4f	2.71	-8.031
4g	2.29	-7.735
4h	2.33	-7.892
4i	2.72	-8.047

4.5 DNA binding studies of the pyrazolone based chromophores

The binding characteristics of metal complexes with DNA could be emphasized by employing electronic spectroscopy. It was revealed from absorption spectra of ligand **2** and its metal complexes 4a-i, in the presence and absence of SS Fish Salmon Sperm did not showed appreciable interaction that is why they were not taken in account.

4.6 UV-Visible of pyrazolone based chromophores 6 and 8a-i.

The absorption maxima (λ_{max}) of ligand (6) and its metal complexes (8a-i) were recorded in DMSO and were shown in Table 5 could be supported with Fig. 8. They showed absorption maxima in the range of 300 to 400 nm which was due to π-π* transition in N=O which due to tautomerism in Nitroso-Oxime. The absorption band between 500 to 700 nm was due to the n- π* transition. All the chromophores had the same functionality but the difference lied in the substituents present at the p-methyl phenyl ring attached to the pyrazol moiety. There was a marked effect on λ_{max} furthermore prominent shifts (bathochromic and hypsochromic) on the λ_{max} were observed on metal complexation. 8a, 8b, 8c and 8h constituted n- π* transitions while the remaining compounds exhibited π-

π* transition. In the prior case bathochromic shift was obvious which was due to increased electron density on the ligand moiety. The reduction the band gap between ground and excited state resulted in the lower energy for the excitation of electrons which corresponded to the bathochromic shift. The bathochromic shift was also designated as the red shift. While the hypsochromic shift was termed as blue shift. In later case i.e 6, 8d, 8e, 8g, 8h the red shift is of less magnitude as compared to the aforesaid. For instance the ligand **6** had the 09 nm red shift which was due to the additional methyl groups present on the phenyl ring as compared to the ligand 2. This electron donating behavior through no bond resonance or hyperconjugation which showed 9 nm Red Shift for 6. The slope ratio curve was given in Fig. 9 for 8a which exhibited the octahedral geometery of the complex.

Table-5: Physical properties of chromophores 6 and complexes 8a-i.

Compounds	Molecular Formula	Molecular Mass	Solution Color in (DMSO)	λ_{max} (nm)
6	$C_{11}H_{12}N_3O_2$	218	Yellow	405/1.094
8a	$Mn(C_{11}H_{12}N_3O_2)_3$	489	Green	586/0.86
8b	$Fe(C_{11}H_{12}N_3O_2)_3$	490	Greenish Yellow	685/0.40
8c	$Co(C_{11}H_{12}N_3O_2)_3$	493	Brownish Green	736/0.36
8d	$Ni(C_{11}H_{12}N_3O_2)_3$	493	Light Green	588/0.35
8e	$Cu(C_{11}H_{12}N_3O_2)_3$	497	Greenish Yellow	416/1.06
8f	$Zn(C_{11}H_{12}N_3O_2)_3$	499	Yellow	436/0.96
8g	$Cd(C_{11}H_{12}N_3O_2)_2$	556	Light Yellow	532/0.32
8h	$Hg(C_{11}H_{12}N_3O_2)_2$	635	Red	734/0.31
8i	$Pd(C_{11}H_{12}N_3O_2)_2$	540	Brownish Yellow	449/0.92

Table-6: Stochiometeric ratios for ligand 6 with metals 7a-i

Sr. No.	Chromophore	Metals	Metal ligand Ratio	Geometery
1	**8a**	Mn^{2+}	1:3	Octahedral
2	**8b**	Fe^{2+}	1:3	Octahedral
3	**8c**	Co^{2+}	1:3	Octahedral
4	**8d**	Ni^{2+}	1:3	Octahedral
5	**8e**	Cu^{2+}	1:3	Octahedral
6	**8f**	Zn^{2+}	1:3	Octahedral
7	**8g**	Cd^{2+}	1:2	Tetrahedral
8	**8h**	Hg^{2+}	1:2	Tetrahedral
9	**8i**	Pd^{2+}	1:2	Square planer

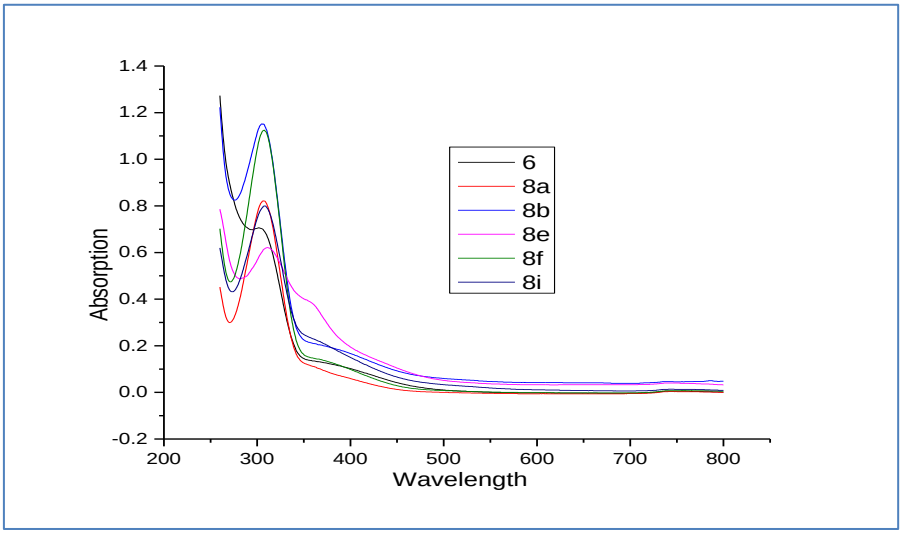

Fig-8: UV-Visible spectrum of 6 and 8a-i

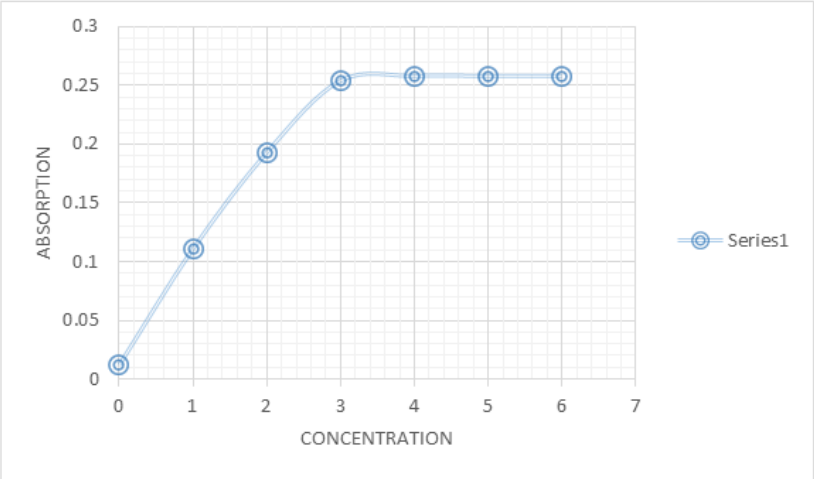

Fig-9: Slope Ratio curve for complex 8a.

4.7 FT-IR studies of pyrazolone based chromophores 6 and 8a-i.

The data for the 2nd series of metal complexes of pyrazolone was given below and could be supported by the Fig. 10 and Fig. 11. The infrared spectra of synthesized ligand and its metal complexes possessed absorption peaks due to O-H (str.3520 cm^{-1}), Ar-H (str.3140 cm^{-1}), C-H (str.2919 cm^{-1}), C=C(str.1611-1684 cm^{-1}), C=O(str.1712 cm^{-1}), N=O(str.1507-1594 cm^{-1}), C-O (str.1367-1409 cm^{-1}), C-N (str.1062 cm^{-1}), C-H (bend.1124-1196 cm^{-1}), M-O (str.511 cm^{-1}) stretching and bending vibrations. O-H (3425 cm^{-1}) as is present in the Fig. 10 corresponded to the hydrogen bonding in the ligand molecules. This was attributed to the fact that the ligand molecules possess keto-oxime tautomerism, where the oxime functionality took part in hydrogen bonding. Keeping in view the spectra of compound 6 given in Fig. 10 the absorption peak at 3520 cm^{-1} was due to O-H group. A phenyl group was connected with nitrogen in the pyrazol moiety whose C-H stretching vibrations were at 3140 cm^{-1}. The stretch at 2656 cm^{-1} is ascribed to the C-H stretch for methyl group present on the phenyl ring para to the pyrazole motif. C=O stretch usually lied in the range of 1715-1745 cm^{-1}, but it is observed at 1712 cm^{-1}. This was actually due to the phenyl ring which reduced the force constant of carbonyl functionality. The bending vibrations of methyl group were present at 1196 cm^{-1}. Synthesis of the ligand (6) and its metal complexes 8a-i were confirmed by FT-IR spectroscopy. The confirmation of the complexation was made on the basis of absorption frequencies at lower wavenumber in the range of 500-550 cm^{-1} for M-O bonding. These were not present in the spectra of 6. One of the representative spectra for 8h was given below in Fig. 11 in which the absorption peak for M-O bond appeared at 511 cm^{-1}.

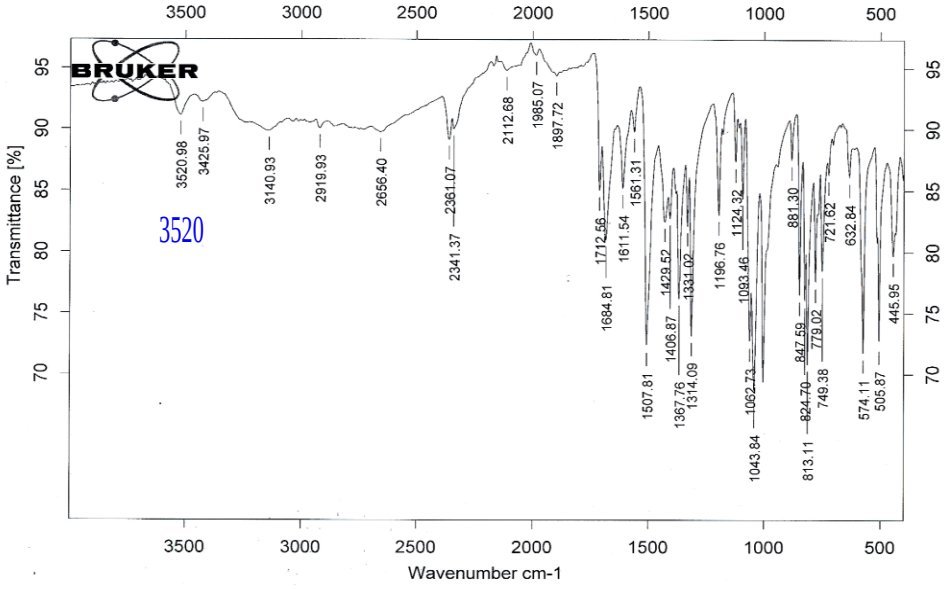

Fig-10: FT-IR spectrum of 6

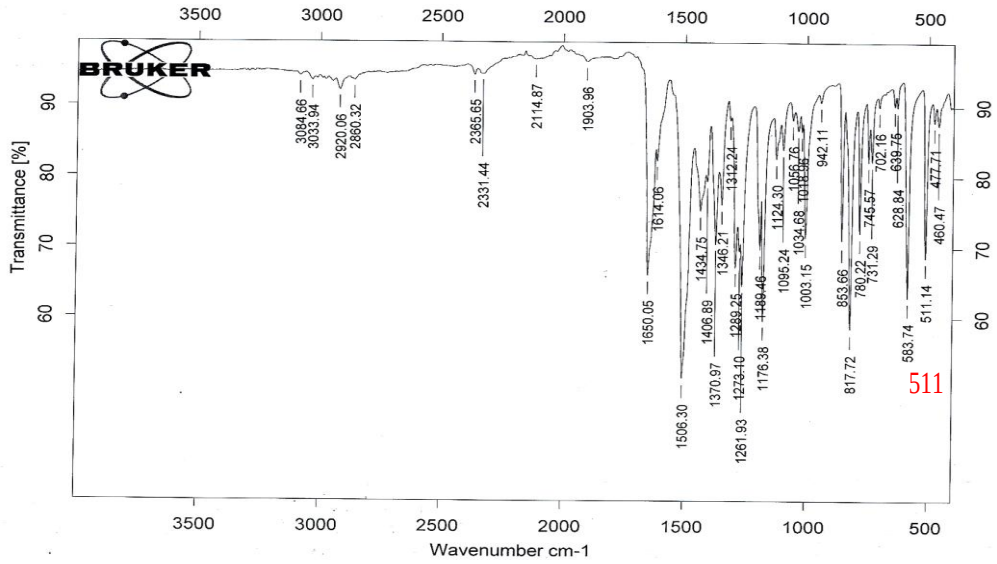

Fig-11: FT-IR spectrum of 8h

4.8 ^{1}H-NMR and ^{13}C-NMR spectroscopic elucidation of 6 and 8a-i

The ^{1}H-NMR and ^{13}C-NMR spectra of 6 was given in the Fig. 12 and 13 respectively. The ^{1}H-NMR spectrum of the ligand 6 exhibited five different kinds of chemically non-equivalent protons. Two signals were present at 2.24 and 2.34 ppm. These two signals were due to the phenomena of keto-oxime tautomerism which was present in the ligand 6. Similarly the signal present at 2.44 ppm was due to the methyl protons present at the phenyl substituted at the p-position. While the signals for aromatic ring were present in the de-shielded region in the range of 7.20-7.73 ppm. The splitting pattern of the aromatic protons was showing that the o-protons were not only chemically equivalent but were also magnetically equivalent and showing their chemical shift at 7.71 (d). This doublet was due to the neighboring protons present at the m-position. Similarly protons present at m-position of the aromatic ring were also showing the doublet signal at 7.22 ppm. More specifically speaking, o-and m-protons were mutually coupled having coupling constant value (J=8.4). In the ^{13}C-NMR of the ligand 6 aromatic peaks were present in the range of 118-128 ppm as were apparent from the Fig. 13. While the signals at 10.98 and 16.04 ppm were for methyl protons present on the pyrazol moity. Ipso-facto methyl protons present at the p-position of the phenyl ring were showing their signals at 19.58 ppm. Similarly ^{13}C signal for C=O was obvious at 160 ppm. While for metal complexes the paramagnetic behavior of metal ions was responsible to distort the ^{1}H-NMR and ^{13}C-NMR and they cannot be considered over here.

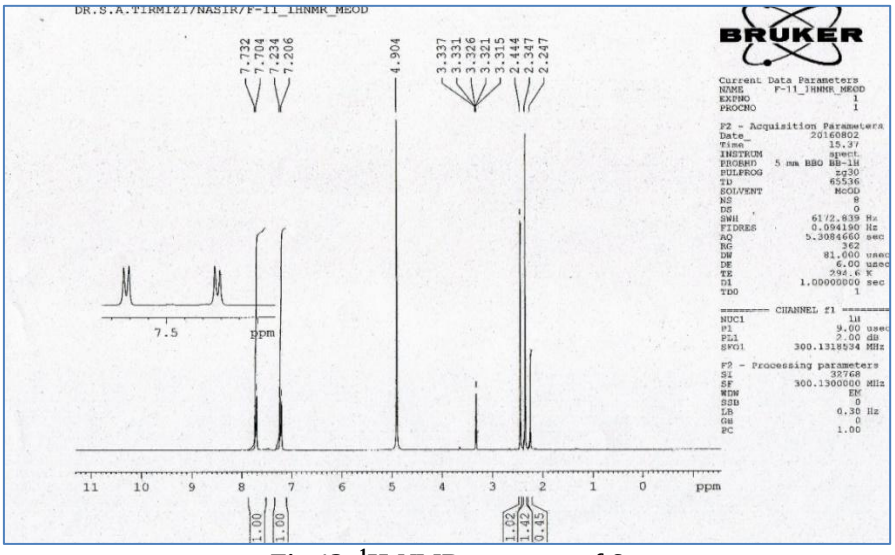

Fig-12: ^{1}H-NMR spectrum of 6

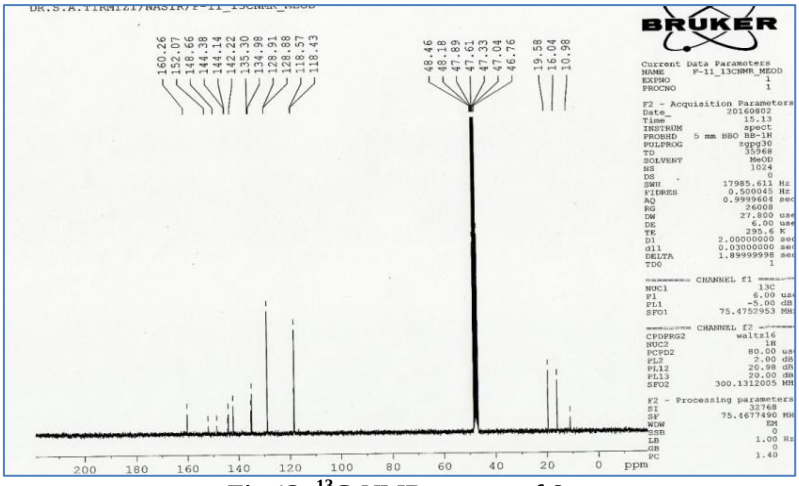

Fig-13: ^{13}C-NMR spectra of 6.

4.9 Electrochemical studies of the 6 and 8a-i.

Cyclic voltammetry was employed for the electrochemical characterization of the synthesized ligand 6 and 8a-i complexes as shown in Fig. 14. The supporting electrolyte was 0.1 M $TBAPF_6$ in DMSO. With the help of this technique the redox potentials i.e HOMO (highest occupied molecular orbitals) and LUMO (lowest unoccupied molecular orbitals) along with energy band gaps (Eg) were calculated.

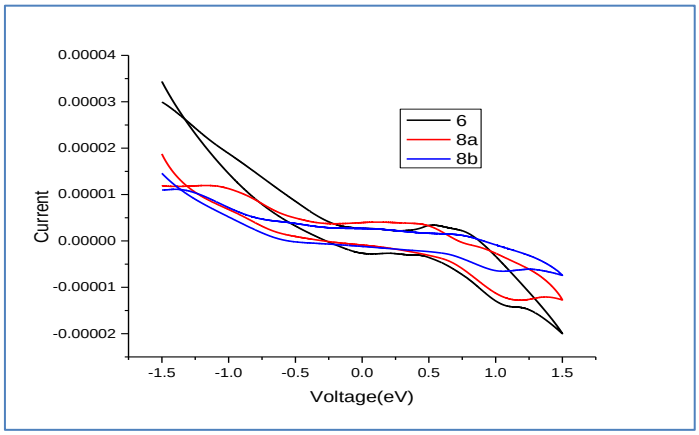

Fig-14: Cyclic Voltammogram of 6 and 8a-i

4.9.1 Lowest Unoccupied Molecular Orbital (LUMO)

Absolute energies of the LUMO levels with respect to the vacuum level were calculated, the redox data were standardized with ferrocenne/ferricinium couple having energy -4.8 eV. The data is given in Table 7 related to LUMO level energies. The LUMO energy levels are in the range of -5.325 to -5.69 eV. It is obvious from the data that 8e contain the central metal ion which has less electronegativity value on Pauling scale (1.90) whose impact is electron donating to the motif due to which the energy of the LUMO levels is decreased. While this is not the case with 8i whose central metal ion has more electronegativity value than Pauling scale (2.20) whose impact is electron withdrawing from the motif due to which the energy of LUMO levels was increased. Increased conjugation or delocalization of electrons decreases the energy difference in the LUMO levels and vice versa.

Table-7: LUMO energy levels of chromophores 6 and 8a-i

Sr. No.	$E_{1/2}$(V)	LUMO (eV)
6	+0.8085	-5.6085
8a	+0.795	-5.595
8b	+0.595	-5.395
8c	+0.556	-5.370
8d	+0.540	-5.355
8e	+0.89	-5.69
8f	+0.82	-5.621
8g	+0.71	-5.526
8h	+0.66	-5.440
8i	+0.525	-5.325

4.9.2 Band Gap Energy (Eg)

The optical band gap energies were calculated using standard procedure. Every solid had its own characteristic energy band structure. This variation in band structure was responsible for the wide range of electrical properties observed in various materials [28].

Band gap energy lies in the range of 1.50 to 2.43 eV. Band gap energies were found to be low for **8i** and high for chromophore **8b**. This contradiction arose due to the involvement of Pd metal which had some kind of electron releasing or back donation effect which increaesed the electron density on the ligand moiety. This caused the decrease in the band gap energy in 8i while this was not the case with 8b. Furthermore due to the involvement of complete by filled 4d orbital which caused the increase in shielding constant. So less effective nuclear charge which enable the metal ion to snatch the electron density from the ligand. This was the reason which made the Palladium to follow back donation contributing to the overall electron releasing effect. Ipso-Facto this was not the case with Fe^{2+} in 8b.

4.9.3 Highest Occupied Molecular Orbitals

The data related to the highest occupied molecular orbitals was given in Table 8 which was calculated by making the use of Bredas equation. The energy lied in the range -7.15 to -7.95 for HOMO. The energy levels for 8a were of high while these were of low for 8e. This discrepancy in energy attributed to the fact that metal ions responsible for dragging the electron density from ligand molecules due to which HOMO energy levels were increased for the complexes. The maximal increment was observed in case of 8a as compared to other metal ions and ligand 8e as presented below in Table 8. This difference showed that the bonding in case of 8a was weaker as compared to 8e. These observations revealed the trend that bonding became stronger from Mn to Cu in the period. This beauty of bond strength could be ascribed to the fact of scandide contraction which went from Fe^{2+} to Cu^{2+}. While the bonding strength mode decreased from top to bottom in IIB i.e Zn to Hg as obvious from the data for 8f, 8g and 8h [23-28].

Table-8: HOMO energy levels and band gap energy of chromophores 6 and 8a-i

Sr. No.	Eg(V)	HOMO (eV)
6	1.84	-7.45
8a	1.56	-7.15
8b	2.43	-7.82
8c	2.36	-7.89
8d	2.11	-7.93
8e	2.26	-7.95
8f	1.92	-7.55
8g	1.89	-7.17
8h	1.63	-7.05
8i	1.50	-6.825

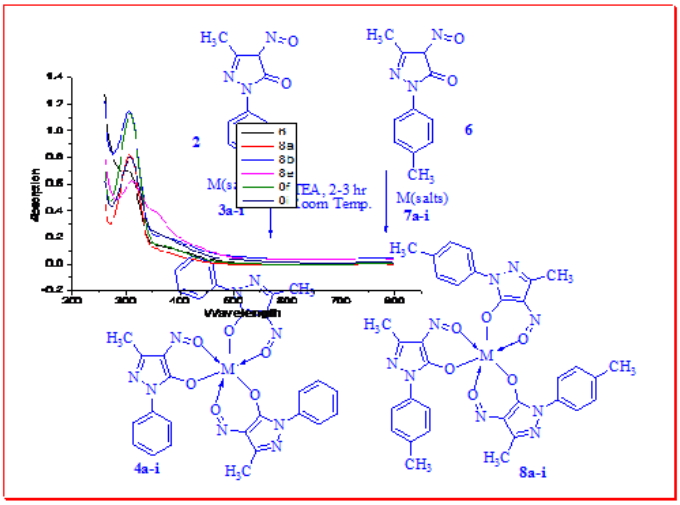

4.10 Anticancer studies

The second series of pyrazolones were screened against Hep G2 cancer cell line. Compound 6 and 8e showed promising results. This was attributed to the planarity of both 6 and 8e. This was evidenced by the good DNA interaction producing excellent spontaneity of the reaction.

4.11 CONCLUSIONS

The synthesis of Nitrosopyrazolones and their metal complexes were conducted in good yields by facile route. Compound 6 (p-methyl 1-phenyl-3-methyl-4-nitroso pyrazolone) and 8e [Bis-p-methyl 1-phenyl-3-methyl-4-nitroso pyrazolone copprate-(II)] showed good anticancer activity against HepG2 cancer cell line.

REFERENCES

1. Kuncheria, B., & Indrasenan, P. (1988). Thorium (IV) nitrate complexes with some substituted pyrazol-5-ones.
2. Agarwal, R. K., & Arora, K. (1993). Synthesis and Characterization of Thoriuti (IV) Adducts of Some Pyrazolone Ligands. Synthesis and Reactivity in Inorganic and Metal-Organic Chemistry, 23(4), 653-670.
3. Agarwal, R. K., & Arora, K. (1993). Synthesis and characterization of dioxouranium (vi) complex of pyrazolones ligands. Polish journal of chemistry, 67(1), 25-32.
4. Sorenson, J. R. (1989). 6 copper complexes offer a physiological approach to treatment of chronic

diseases. Progress in medicinal chemistry, 26, 437-568.
5. Lewis, J. A. S. (2007). Heterocyclic metal-binding groups for matrix metalloproteinase and anthrax lethal factor inhibition. University of California, San Diego.
6. Maurya, R. C., Mishra, D. D., Rao, N. S., & Rao, N. N. (1992). Synthesis and characterization of some ruthenium (II) Schiff base complexes derived from 1-phenyl-3-methyl-4-benzoyl-5-pyrazolone. Polyhedron, 11(22), 2837-2840.
7. Christianson, D. W. (1991). Structural biology of zinc. Advances in protein chemistry, 42, 281-355.
8. Williams, R. J. (1982). Metal ions in biological catalysts. Pure and Applied Chemistry, 54(10), 1889-1904.
9. Bonomo, R. P., Tabbi, G., Santoro, A. M., Conte, E., & Marchelli, R. (1994). O2− scavenger properties of copper (II) complexes with diamino-diamide-type ligands. Journal of inorganic biochemistry, 53(2), 127-138.
10. Norris, G. E., Anderson, B. F., & Baker, E. N. (1986). Blue copper proteins. The copper site in azurin from Alcaligenes denitrificans. Journal of the American Chemical Society, 108(10), 2784-2785.
11. Cleare, M. J. (1974). Transition metal complexes in cancer chemotherapy. Coordination Chemistry Reviews, 12(4), 349-405.
12. Das, M., & Livingstone, S. E. (1976). Metal chelates of dithiocarbazic acid and its derivatives. IX. Metal chelates of ten new Schiff bases derived from S-methyldithiocarbazate. Inorganica Chimica Acta, 19, 5-10.
13. Ali, M. A., & Bose, R. N. (1984). Transition metal complexes of furfural and benzil schiff bases derived from S-benzyldithiocarbazate. Polyhedron, 3(5), 517-522.
14. Patel, D. R., Patel, N. B., Patel, B. M., & Patel, K. C. (2014). Synthesis and dyeing properties of some new monoazo disperse dyes derived from 2-amino-4-(2′, 4′-dichlorophenyl)-1, 3 thiazole. Journal of Saudi Chemical Society, 18(6), 902-913.
15. Hussain, G., Abbas, N., Ather, M., Khan, M. U. A., Saeed, A., Saleem, R., & Shabir, G. (2016). Synthesis of 1- (p- Sulphophenyl)- 3- methyl- 5- pyrazolone Based Acid Dyes and Their Applications on Leather. Journal of the Chinese Chemical Society, 63(8), 645-652.
16. Maurya, R. C., Mishra, D. D., Rao, N. S., & Rao, N. N. (1992). Synthesis and characterization of some ruthenium (II) Schiff base complexes derived from 1-phenyl-3-methyl-4-benzoyl-5-pyrazolone. Polyhedron, 11(22), 2837-2840.
17. Abbas, N., Tirmizi, S. A., Shabir, G., Saeed, A., Hussain, G., Channer, P. A., ... & Ayaz, M. (2018). Chromium (III) complexes of azo dye ligands: Synthesis, characterization, DNA binding and application studies. Inorganic and Nano-Metal Chemistry, 48(1), 57-66.
18. Covaci, A., Dirtu, A. C., Voorspoels, S., Roosens, L., & Lepom, P. (2010). Sample preparation and chromatographic methods applied to congener-specific analysis of polybrominated diphenyl ethers. Brominated Flame Retardants, 55-94.
19. Parikh, P. M., & Shah, J. R. (1985). Studies on Six-Coordinate Octahedral Chromium (III) Chelates with Schiff Bases Derived from 4-Acetyl-3-methyl-1-(3′-chloro Phenyl)-2-pyrazolin-5-one. Synthesis and Reactivity in Inorganic and Metal-Organic Chemistry, 15(6), 769-778.
20. Abbas, N., Shabir, G., Saeed, A., Tirmizi, S. A., Echeverría, G. A., Piro, O. E., & Erben, M. F. (2020). Synthesis and Structure of 4-Chloro-2-{[5-(diethylamino)-2-hydroxybenzylidene] amino} phenol and Its Metal Complexes. Russian Journal of General Chemistry, 90(12), 2376-2380.
21. Rana, M., Cho, H. J., Roy, T. K., Mirica, L. M., & Sharma, A. K. (2018). Azo-dyes based small bifunctional molecules for metal chelation and controlling amyloid formation. Inorganica chimica acta, 471, 419-429.
22. de Faria, R. C., Vila-Nova, L. G., Bitar, M., Resende, B. C., Arantes, L. S., Rebelato, A. B., ... & de Oliveira Lopes, D. (2016). Adenine glycosylase MutY of Corynebacterium pseudotuberculosis presents the antimutator phenotype and evidences of glycosylase/AP lyase activity in vitro. Infection, Genetics and Evolution, 44, 318-329.
23. Marchetti, F., Pettinari, R., & Pettinari, C. (2015). Recent advances in acylpyrazolone metal complexes and their potential applications. Coordination Chemistry Reviews, 303, 1-31.
24. Gouda, M. A., Eldien, H. F., Girges, M. M., & Berghot, M. A. (2016). Synthesis and antitumor evaluation of thiophene based azo dyes incorporating pyrazolone moiety. Journal of Saudi Chemical Society, 20(2), 151-157.
25. Nair, M. S., Arish, D., & Johnson, J. (2016). Synthesis, characterization and biological studies on some metal complexes with Schiff base ligand containing pyrazolone moiety. Journal of Saudi Chemical Society, 20, S591-S598.
26. Geng, J., Xu, D., Chang, F. F., Tao, T., & Huang, W. (2017). From heterocyclic hydrazone to hydrazone-azomethine dyes: Solvent and pH induced hydrazone and azo-keto transformation for a family of pyrazolone-based heterocyclic dyes. Dyes and Pigments, 137, 101-110.
27. Rizk, H. F., Ibrahim, S. A., & El-Borai, M. A. (2017). Synthesis, dyeing performance on polyester fiber and antimicrobial studies of some novel pyrazolotriazine and pyrazolyl pyrazolone azo dyes. Arabian Journal of Chemistry, 10, S3303-S3309.
28. Kandhasamy, S., Ramanathan, G., Muthukumar, T., Thyagarajan, S., Umamaheshwari, N., Santhanakrishnan, V. P., & Perumal, P. T. (2017). Nanofibrous matrixes with biologically active hydroxybenzophenazine pyrazolone compound for cancer theranostics. Materials Science and Engineering: C, 74, 70-85.